SWCX Emission from the Helium Focusing Cone – Model to Data Comparison

D. Koutroumpa,[1,2] M. R. Collier,[3] K. D. Kuntz,[4] R. Lallement,[2]
and
S. L. Snowden[1]

ABSTRACT

A model for heliospheric solar wind charge exchange (SWCX) X-ray emission is applied to a series of *XMM-Newton* observations of the interplanetary focusing cone of interstellar helium. The X-ray data are from three coupled observations of the South Ecliptic Pole (SEP, to observe the cone) and the Hubble Deep Field-North (HDFN, to monitor global variations of the SWCX emission due to variations in the solar wind) from the period 24 November to 15 December 2003. There is good qualitative agreement between the model predictions and the data with the maximum SWCX flux observed at an ecliptic longitude of $\sim 72°$, consistent with the central longitude of the He cone.

We observe a total excess of 2.1 ± 1.3 LU in the O VII line and 2.0 ± 0.9 LU in the O VIII line. However, the SWCX emission model, which was adjusted for solar wind conditions appropriate for late 2003, predicts an excess from the He cone of only 0.5 LU and 0.2 LU, respectively, in the O VII and O VIII lines. We discuss the model to data comparison and provide possible explanations for the discrepancies.

We also qualitatively reexamine our SWCX model predictions in the $\frac{1}{4}$ keV band with data from the *ROSAT* All-Sky Survey towards the North and South Ecliptic Poles, when the He cone was probably first detected in soft X-rays.

Subject headings: X-rays: observations — Solar System

1. Introduction

Solar wind charge exchange (SWCX) X-ray emission in the heliosphere originates when a high charge state ion of the solar wind interacts with a neutral atom and gains an electron in a highly excited state which then decays by emission of an X-ray with a characteristic energy of the ion. SWCX emission occurs over a wide range of spatial scales including comets (where such emission was first conclusively observed, e.g., Lisse et al. 1996), the near-Earth environment where the neutrals are exospheric material in and near the magnetosheath (e.g., Cravens et al. 2001; Snowden et al. 2009), and throughout the solar system where the target atoms are from the interstellar medium (e.g., Cox 1998; Cravens 2000; Smith et al. 2005). SWCX emission comprises a significant part of the diffuse X-ray background observed at energies $\lesssim 1$ keV, and can be both a signal of interest in studies of the solar system or an unfortunate contamination component in studies of the hot, diffuse plasmas in the Milky Way and beyond.

In theory, SWCX emission exhibits very distinct spectral characteristics with respect to thermal plasma emission. For instance, the line intensity ratios in triplets of the He-like ions O VII and

[1]Code 662, NASA/Goddard Space Flight Center, Greenbelt, MD 20771

[2]Service d'Aéronomie, UMR 7620, CNRS, Université de Versailles Saint-Quentin, BP3, 91371 Verrières-le-Buisson, France

[3]Code 673, NASA/Goddard Space Flight Center, Greenbelt, MD 20771

[4]Henry A. Rowland Department of Physics and Astronomy, The Johns Hopkins University, 366 Bloomberg Center, 3400 N. Charles Street, Baltimore, MD 21218

Ne IX are very different and could be used as spectral diagnostics to separate the two mechanisms (e.g., Lallement 2008, and references therein). Future missions which include non-dispersive microcalorimeter spectrometers will be able to separate thermal from SWCX emission using the triplets (e.g., Snowden 2008). However for diffuse sources, with the spectral resolution of current missions it is impossible, in general, to distinguish individual SWCX X-rays from those with a more distant origin, and alternative diagnostic information must be used to separate the components of the X-ray background. Temporal variation can be used to a certain extent depending on the length of an observation, and indeed this method was used in cleaning the *ROSAT* All-Sky Survey (RASS, Snowden et al. 1997). SWCX emission from the near-Earth environment will track relatively well variations in the solar wind flux as measured by the Advanced Composition Explorer (*ACE*, Stone et al. 1998) and *WIND* (Ogilvie et al. 1995) instruments. However, identifying and modeling a temporally variable component can only address a fraction of the SWCX emission. Emission from interactions with interstellar (IS) neutrals drifting through the solar system will typically have minimal temporal variation as the observed flux along any line of sight is an integral over weeks of solar wind conditions. Because of the long (relative to a typical X-ray observation) times of any expected variation, IS SWCX effectively contributes a zero-level offset to observations of the diffuse X-ray background of more distant origin.

While there are models for SWCX emission from the heliosphere, testing them is problematic. Koutroumpa et al. (2007), using a self-consistent model of the heliospheric SWCX emission, managed to associate observed discrepancies in *XMM-Newton* and *Suzaku* observations separated by several years with solar cycle-scale variations. A recent paper (Snowden et al. 2009) was relatively successful at using an *XMM-Newton* observation to test a model (Robertson & Cravens 2003) for emission from the near-Earth environment. In this paper we use a different series of *XMM-Newton* observations to search for emission from the solar system. Specifically, we use multiple observations of the south ecliptic pole as Earth passes over the the ISM helium focusing cone downstream of the Sun to search for a correlation with the expected variation from the model.

2. Observations

2.1. Helium Focusing Cone

The flow of interstellar neutrals through the solar system is due to the motion of the heliosphere at about 25 km s^{-1} through the local IS cloud (LIC). This material, a gas of mostly hydrogen atoms with about 15% helium flows from the direction of $\lambda, \beta \sim 252°, 9°$ ($\alpha, \delta \sim 252°, -14°$). This places the Earth upstream of the Sun in the interstellar neutral flow in early June and downstream in early December every year (Gruntman 1994). Although both radiation pressure and gravity affect the hydrogen trajectories (e.g., Quémerais et al. 1999; Lallement 1999), only gravity significantly affects the helium trajectories which execute Keplarian orbits and form a "focusing cone" downstream of the sun, resulting in a localized downstream enhancement of helium observed annually by Earth orbiting and L1 spacecraft (Bzowski et al. 1996; Frisch 2000).

Many diverse sets of observations have confirmed this helium focusing cone phenomenon, and have put strict constraints on the helium flow parameters (density, temperature, velocity vector), including direct neutral gas measurements (Witte 2004) and UV backscattering (Lallement et al. 2004; Vallerga et al. 2004) as well as pickup ions (Gloeckler et al. 2004) which form when the neutral helium becomes ionized primarily from solar photons and subsequently "picked-up" by the solar wind flow (Moebius et al. 1985). Of these, pickup ions have been particularly useful because they display a clear spectral signature, a cut-off at two times the solar wind speed resulting from their low initial speed (~25 km/s) in comparison to the solar wind speed (~400 km/s). However, their low count rates also necessitate aggressive averaging, commonly 30-day running averages, to smooth out fluctuations.

Recently, Collier et al. (2004), based on an analysis of several diverse data sets, proposed the presence of a secondary stream of neutral atoms at 1 AU located at a higher ecliptic longitude by 10 to 40° than the primary stream described above (see also Wurz et al. 2004). These neutrals seem to be far more energetic than the nominal He flow. Very recent observations from the pair of

STEREO spacecraft (Wang et al. 2008) showing two peaks in the 4-20 keV neutral hydrogen atom flux, one primary peak at 245° close to the nominal upstream direction and another secondary peak shifted 16° toward higher ecliptic longitudes than the nominal upstream direction, appear to confirm this prediction. Additionally, Mars Express has observed a neutral atom signal consistent with this secondary stream proposal (Holmström et al. 2008). Nevertheless, all observations of slow neutrals show only one cone, and the secondary cone, should it exist, must consist of high velocity neutrals which are not well focused.

Because high charge state solar wind ions will charge exchange with the enhanced helium in the downstream region emitting soft X-rays, the helium focusing cone should be observable in soft X-rays (Cravens et al. 2001). Indeed, the *ROSAT* All-Sky Survey (RASS) data (Snowden et al. 1995) when observing within two degrees of the south ecliptic pole show enhanced emission in early December (see §2.4) with some evidence for a secondary peak about ten days later (or ten degrees higher in ecliptic longitude) than the expected location of the helium focusing cone (see Figure 5). These *ROSAT* data in part motivated the *XMM-Newton* observations of the helium focusing cone and particularly the day of year of the third observation.

2.2. X-ray Data

Three pairs of *XMM-Newton* calibration observations, matched pointings of the south ecliptic pole (SEP, to observe the focusing cone) and of the Hubble Deep Field – North (HDFN), were approved by the project and scheduled for late 2003 (see Table 1 for the observation details). The coupled observations of the HDFN were included to serve as controls to monitor the SWCX emission variation not associated with the focusing cone (e.g., due to variations in the solar wind flux and composition) which could arise from Earth's magnetosheath or more generally from the heliosphere.

The orbit of *XMM-Newton* is highly elongated (perigee $\sim 10^4$ km, apogee $\sim 10^5$ km) and inclined (inclination $\sim -40°$) relative to the equatorial plane. In late November and early December, the time period when Earth is closest to the focusing cone and therefore the time for these observations, the apogee lies in the anti-solar direction. This is fortuitous for two reasons: since observations take place away from perigee any observed SWCX emission from the magnetosheath (well down the flanks of the magnetosheath and away from the sub-solar point) is significantly reduced (e.g., Robertson & Cravens 2003) and the likelihood of soft proton contamination is also reduced (Kuntz & Snowden 2008).

We reduced the EPIC data using the *XMM-Newton* ESAS[1] analysis package (Snowden & Kuntz 2006) as demonstrated in Snowden et al. (2008). The data were first screened for variations in the light curve which removed excesses in the normal internal particle background and more commonly contamination by soft protons (Kuntz & Snowden 2008). Next, data from the full field of view were extracted after the exclusion of point sources to a limit to 10^{-14} ergs cm^{-2} s^{-1}. Finally model particle background spectra were produced for subtraction during the spectral fitting process.

After extraction the spectra were then fit using a model which included two thermal components (an unabsorbed ~ 0.1 keV model for local emission and an absorbed ~ 0.3 keV model for the more distant disk and halo emission) and an absorbed power law representing the cosmic background, monochromatic lines at 1.49 keV and 1.75 keV representing the internal fluorescent Al Kα and Si Kα background, and a power law not folded through the instrumental response representing any residual soft proton contamination left after the screening process. Xspec APEC thermal spectral models with variable abundances were used where the abundance of oxygen was set to zero and the other abundances were fixed at 1 (based on the assumption that oxygen will dominate any SWCX emission in the *XMM-Newton* bandpass). Monochromatic lines at 0.57 keV and 0.65 keV were added to the model to represent the observed oxygen emission from both SWCX and more distant cosmic emission, the latter which produces a constant contribution. The absorption of the halo thermal components and the power law were fixed at the Galactic values. Two other monochromatic lines were also added, C VI at 0.46 keV and another O VIII line at 0.81 keV. The addition of the C VI line marginally improved the fit but left the χ^2_ν value unchanged with detections

[1] http://heasarc.gsfc.nasa.gov/docs/xmm/xmmhp_xmmesas.html

TABLE 1

XMM-Newton OBSERVATION DETAILS AND FITTED LINE FLUXES IN LU

ObsId	Observation Start	α	δ	Exposure	Good Time	Fitted O VII Flux	Fitted O VIII Flux
0162160101	2003-11-24 20:07:55	06 00 09.36	-66 34 15.7	13.44 ks	11.90 ks	8.3±0.5	3.8±0.2
0162160201	2003-11-24 09:18:35	12 37 01.02	62 12 57.1	15.25 ks	12.89 ks	8.9±0.6	4.3±0.4
0162160301	2003-12-05 20:47:15	06 00 07.63	-66 34 26.8	11.45 ks	8.57 ks	9.7±0.7	4.1±0.4
0162160401	2003-12-06 12:38:23	12 37 01.02	62 13 06.2	10.85 ks	9.62 ks	8.0±0.6	2.1±0.3
0162160501	2003-12-14 14:26:09	06 00 06.48	-66 34 34.8	11.45 ks	9.32 ks	8.6±0.7	3.5±0.4
0162160601	2003-12-14 23:15:09	12 37 01.70	62 13 16.0	43.17 ks	10.06 ks	7.0±0.5	1.8±0.3
0111550201	2001-05-18 22:17:34	12:36:50.00	62:13:12.0	41.88 ks	34.89 ks	10.4±0.5	2.6±0.2
0111550401	2001-06-01 08:16:36	12:36:57.00	62:13:30.0	91.99 ks	26.73[a] ks	8.8±0.5	2.8±0.3

[a]Data from the low SWCX emission part of the observation

at the $< 2\sigma$ level. The O VIII line at 0.81 keV was insignificant. A spectrum derived from the *ROSAT* All-Sky Survey (RASS) data was simultaneously fit with the oxygen emission coming from the thermal models rather than the monochromatic lines. (The RASS data primarily constrain the low-temperature thermal component.)

All of the SEP data and all of the HDFN data were fit simultaneously allowing only the SWCX oxygen Gaussians, instrumental Al and Si Gaussians, and soft-proton power law components to vary between observations. The model components representing the cosmic background were assumed to be constant. Table 1 also lists the fitted values for the O VII and O VIII flux in line units (LU, photons cm^{-2} s^{-1} sr^{-1}). Also included are results from the spectral fits from two of the HDFN spectra from Snowden, Collier, & Kuntz (2004). The data are also plotted in Figure 1.

Figure 2 shows the spectral fits of the SEP data (the fits to the HDFN data were similar). The fits are reasonably good for the cosmic background with a χ^2_ν value of 1.24 for 902 degrees of freedom (χ^2_ν value of 1.25 for 771 degrees of freedom for the HDFN data). Of note in the plot are the significantly better statistics of the PN data with the O VII line clearly seen at $E \sim 0.57$ keV and with the O VIII line forming the $E \sim 0.65$ keV hump on the shoulder of the O VII line.

The fitted fluxes as plotted in Figure 1 show significant scatter, and any expected trend of the first SEP (off-cone) pointing being lower while the last two pointings (on-cone, the first at the nominal cone position, the second at the secondary cone position of Collier et al. 2004) being higher is completely obscured. (In fact the general trend is in the opposite direction.) However, the HDFN results which are nearly unaffected (see below) by the helium focusing cone enhancement, and should be roughly constant except for any variation in the solar wind flux, also show the same trend. We therefore used the HDFN data to normalize the SEP data. As noted above, the observations took place while the *XMM-Newton* satellite was on the opposite side of Earth from the Sun minimizing the SWCX emission from in and near the magnetosheath (Robertson & Cravens 2003) allowing the observed SWCX X-ray emission to be dominated by the heliosphere.

With this assumption we used the data from the

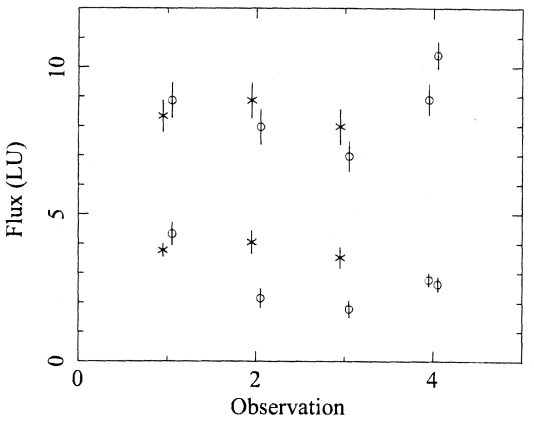

Fig. 1.— Fitted values for the O VII (upper grouping of points) and O VIII line fluxes (lower grouping of points). Data points with an X symbol are in the direction of the SEP and data points with a circle symbol are in the direction of the HDFN. The pairs of points at observations 1−3 are ObsIDs (0162160101, 0162160201), (0162160301, 0162160401), and (0162160501, 0162160601), respectively. The observation 4 data points are from two HDFN spectra (0111550201, 0111550401) from Snowden, Collier, & Kuntz (2004).

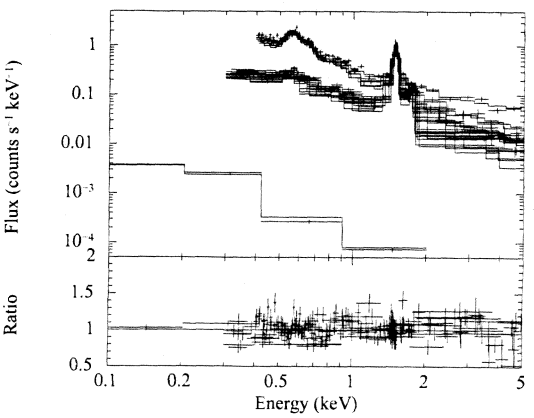

Fig. 2.— Spectral fit for the SEP spectra. The upper set of data and curves are the three PN spectra, the middle set of data and curves are the six MOS1 and MOS 2 spectra, and the bottom is the RASS spectrum.

TABLE 2
NORMALIZED[a] LINE FLUXES IN LU

ObsId	Normalized[b] O VII Flux	Normalized[b] O VIII Flux	Normalized[c] O VII Flux	Normalized[c] O VIII Flux
0162160101	6.5±0.8	1.6±0.3	7.2±0.8	1.7±0.3
0162160301	8.5±1.0	3.4±0.8	9.3±1.0	3.7±0.8
0162160501	8.6±0.7	3.5±0.4	8.6±0.7	3.5±0.4

[a]Data are scaled for the observed variation of the HDFN flux and then normalized by the model HDFN SWCX flux.

[b]Scaled only by the observed variation of the HDFN flux.

[c]Scaled by the observed variation of the HDFN flux and then scaled again by the model variation of the HDFN SWCX flux.

TABLE 3
OFFSET SUBTRACTED AND NORMALIZED[a] LINE FLUXES IN LU

ObsId	Normalized[b] O VII Flux	Normalized[b] O VIII Flux	Normalized[c] O VII Flux	Normalized[c] O VIII Flux
0162160101	2.7±0.6	0.5±0.2	3.0±0.6	0.6±0.2
0162160301	4.5±1.0	1.6±0.7	4.7±1.0	1.8±0.7
0162160501	4.5±0.7	1.8±0.4	4.5±0.7	1.8±0.4

[a]Data are first modified by subtracting half of the minimum observed intensity for each direction and each line and then scaled for the observed variation of the HDFN flux and finally normalized by the model HDFN SWCX flux.

[b]Scaled only by the observed variation of the HDFN flux.

[c]Scaled by the observed variation of the HDFN flux and then scaled again by the model variation of the HDFN SWCX flux.

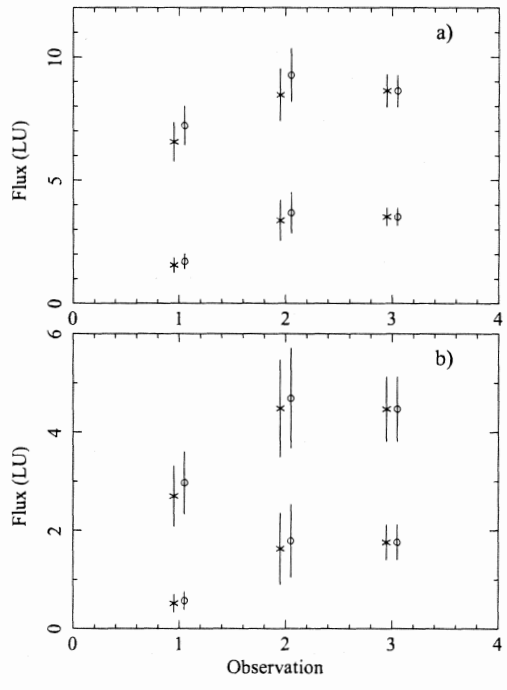

Fig. 3.— a) The SEP line fluxes after using the HDFN data to normalize flux for the O VII (upper grouping of points) and O VIII line fluxes (lower grouping of points). The data are from Table 2. Data points with an X symbol are show the results when the HDFN SWCX flux is assumed to be constant. The points with a circle symbol include a further scaling to account for the model variation in the direction of the HDFN, see text for the details. b) Same as a) except for the assumption that half of the minimum observed flux in both directions (data from Table 3) has an origin outside of the heliosphere.

third observation to scale the data from the first and second observations, with the results listed in Table 2 and plotted in Figure 3a. However, our model prediction for the HDFN SWCX flux does vary by about 10% (see Table 5, and Figure 6) with the intensity being lowest for the last observation. We use these model fluxes to add a second normalization to the SEP fluxes where the results are also listed in Table 2 and plotted in Figure 3a. There are a couple of caveats in using this approach. First, we assume that the heliospheric SWCX oxygen line emission dominates the observed flux. A significant contribution either from the Milky Way or yet more distant emission or a constant flux from the heliopause would decrease the accuracy of the scaling by adding a constant offset. Second, we assume that the solar wind, both flux and abundances, on average are the same for both the northern and southern solar hemispheres.

To gauge the affect of possible more distant emission we recalculated the normalized line intensities with the assumption that half of the minimum observed fluxes in both directions and both spectral lines originates beyond the heliosphere. The results are listed in Table 3 and plotted in Figure 3b. Not surprisingly the sense of the variation is the same as before and the only significant difference is that the fluxes are reduced by the factor of two.

2.3. Solar Wind Data

The *ACE* and *WIND* satellites at the L1 point provide density and velocity (among other quantities) measurements of various species in the solar wind. Since SWCX emission is proportional to the flux of the solar wind species producing the emission, the *ACE* and *WIND* data can be used to gain insight into the variation of the observed flux. Figure 4 shows the solar wind proton flux and the O^{+7}/O^{+6} density ratio for the period of this program (the observation intervals are shown by the vertical lines).

Both the solar wind proton flux and the oxygen density ratio show significant but not unusual variations over the interval. It is unfortunate that the data which are the most relevant, the actual O^{+8} and O^{+7} fluxes, are not readily available from the *ACE* instruments and the two displayed parameters must act as surrogates for at least a qual-

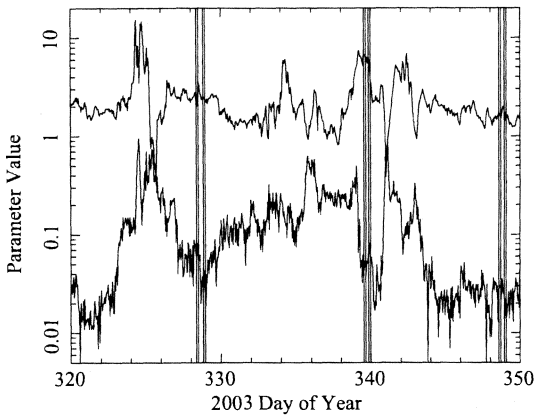

Fig. 4.— *ACE* solar wind proton flux (upper curve, units of 10^8 particles cm^{-2} s^{-1}) and the O^{+7}/O^{+6} density ratio data (lower curve) covering the time interval of the observations. The vertical lines show the individual observation intervals.

itative understanding of the circumstances. Note that both the solar wind flux and primarily the O^{+7}/O^{+6} density ratio are lower in the days leading up to the third observation group than the similar periods before first and second observation groups. This supports the reasonableness for scaling the fitted O VII and O VIII fluxes.

2.4. *ROSAT* All-Sky Survey Ecliptic Pole Data

In addition to the *XMM-Newton* observations of the He focusing cone we also examined the RASS data from the ecliptic poles. Figure 5 shows the total $\frac{1}{4}$ keV count rate, the Long-Term Enhancement[2] (LTE, Snowden et al. 1997) and LTE-subtracted RASS $\frac{1}{4}$ keV surface brightnesses as a function of day of year for the south and north ecliptic poles (NEP). The data are from periods where the satellite pointing directions were within 2° ofthe poles and are two-day averages. The removal of the LTE enhancements in essence applied a low-pass filter to the data with a time constant on the order of a day. While some of the temporal variation in the "clean" data is possible due

[2]Long-Term Enahncements are the name given to the obvious SWCX enhancements which affected the RASS data. At the time (early 1990's) the origin of this temporally varying "background" enhancement was unknown.

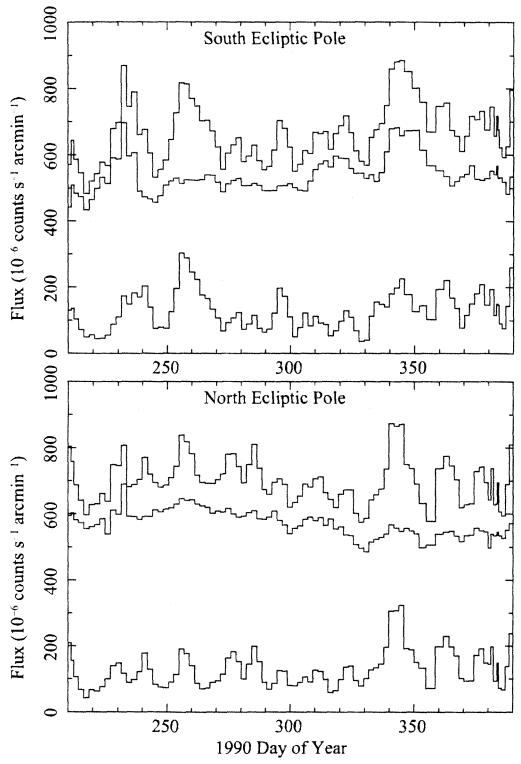

Fig. 5.— *Upper Panel:* Two-day average RASS $\frac{1}{4}$ keV surface brightnesses for the intervals of the scans within 2° of the south ecliptic pole. The lower curve is the LTE surface brightness subtracted from the data (upper curve, Snowden et al. 1997). The middle curve is the "cleaned" (LTE subtracted) RASS surface brightness. *Lower Panel:* Same as the upper panel except the data are from the north ecliptic pole. Note that day 366.0 of 1990 is day 1.0 of 1991.

to variation in the cosmic background of distant origin (i.e., beyond the heliosphere), most is due to variations in the SWCX emission and the variable success in removing it from the RASS. Of note, however, are the enhancements in both the SEP and NEP data near day 345 in the total observed flux and a corresponding enhancement in the cleaned flux for the SEP. These are the strongest enhancements in terms of the integrated magnitude with the southern enhancement being somewhat stronger. Day 345 corresponds to the time period when Earth, and therefore *ROSAT*, were over the central direction of the He cone. The solar wind data in the early 1990s, the time period of the RASS observations (the last half of 1990), are too sparse (see Figure 9) to allow a significant quantitative analysis of the data. However, qualitatively the RASS data are in agreement with a model for enhanced SWCX emission during the period when *ROSAT* observed through the helium focusing cone.

3. SWCX Model description

The heliospheric SWCX model we use for our simulations is extensively described in Koutroumpa et al. (2006, 2007). This model is a self-consistent calculation of the solar wind charge-exchange X-ray line emission for any line of sight (LOS) through the heliosphere and for any observation date, based on 3-dimensional grids of the IS neutral species (H and He) distributions in the heliosphere modulated by solar activity conditions (gravity, radiation pressure, and ionization processes). Highly charged heavy solar wind (SW) ions are propagated radially through these grids and the charge-transfer collision rates are calculated for each of the ion species, including the evolution of their density due to charge-transfer with the IS atoms. With this process, we establish 3-dimensional emissivity grids for each SW ion species, using photon emission yields computed by Kharchenko & Dalgarno (2000) for each spectral line following charge exchange with the corresponding neutral species (H and He individually). Finally, the X-ray line emission is integrated along any LOS and observation geometry (for each observation date) in order to build the complete spectrum of SWCX emission in the given direction. For comparison to present X-ray observations we use the O VII triplet at 0.57 keV and the O VIII line at 0.65 keV, as they are the strongest spectral features and provide the best signal-to-noise ratio for the observations.

We have conducted three simulations for each of the XMM observations that we name Models A, B and C. For all simulations the initial parameters of the IS neutral H and He flows are identical. The parameters specifying the IS neutral hydrogen are: n_H (at 100 AU) = 0.1 cm^{-3}, T = 13 000 K, V_o = 21 km s^{-1}, $\lambda_{UW} = 252.3°$, $\beta_{UW} = 8.5°$ (Lallement et al. 2005), where λ_{UW} and β_{UW} are the helioecliptic longitude and latitude respectively for the upwind direction of the incoming neutral H flow. The IS helium distribution has the following initial parameters: n_{He} (at 100 AU) = 0.015 cm^{-3}, T = 6 300 K, V_o = 26.2 km s^{-1}, $\lambda_{UW} = 254.7°$, $\beta_{UW} = 5.3°$ (Witte 2004; Vallerga et al. 2004; Gloeckler et al. 2004). With those parameters, the He focusing cone is expected to be centered around (λ_{DW}, β_{DW}) = (74.7°, -5.3°). Model A assumes average solar minimum conditions (e.g., years 1996-1997 or 2007-2008), Model B assumes solar conditions typical for late 2003, and Model C assumes average solar maximum conditions (e.g., years 1990 and 2000-2001). The basic differences in the three simulations are the neutral density distributions as they are shaped by the solar activity and ionization processes and the solar wind heavy ion distribution.

The H density reflects the action of gravity, radiation pressure, and losses due to CX collisions with SW protons and solar EUV ionization. The ratio, μ, of radiation pressure to gravity for neutral H varies from 0.9 at solar minimum to 1.5 at solar maximum (Woods et al. 2000). The main source of ionization for H atoms is CX with solar wind protons. Ionization rates are derived as a function of heliographic latitude from the SOHO/SWAN Ly-α preliminary data analysis (Quémerais et al. 2006). For solar minimum the ionization rate decreases at around 40% from the solar equator to the solar poles, with an equatorial value of 6.7×10^{-7} s^{-1}, while in solar maximum the relative decrease from the equator to the poles is only around 15% , with an equatorial value of 8.4×10^{-7} s^{-1}. In late 2003, with $\mu \sim 1.2$, the equatorial ionization rate is 7.5×10^{-7} s^{-1} and the equator to pole relative decrease is 30% in the H ionization rates.

For He atoms the radiation pressure to gravity ratio is effectively zero and the atoms are grav-

itationally focused downwind (the helium focusing cone). The main cause of ionization is solar EUV radiation and electron impact. Recent work has shown strong evidence for a latitudinally anisotropic distribution of the He 30.4 nm solar irradiance and thus of the He photo-ionization rate (Witte 2004; Auchère et al. 2005) and it has also been shown that the electron impact ionization rate is also dependent on heliographic latitude (McMullin et al. 2004). In Koutroumpa et al. (2007) we tested preliminary grids of anisotropic He distributions in our calculation of heliospheric X-rays induced in SWCX collisions. The present study, which examines emission from the He focusing cone, attempts to constrain the He ionization rates and their latitudinal dependance.

For maximum solar activity, the photo-ionization rate is 1.4×10^{-7} s^{-1} at the solar equator, while during solar minimum the photo-ionization rate at the solar equator is 0.7×10^{-7} s^{-1}. The photo-ionization rates present a 50% decrease toward the solar poles. In 2003, the He photo-ionization rate was 1×10^{-7} s^{-1} at the solar equator, again with a 50% decrease at the solar poles.

The radial dependence of electron impact ionization is taken from Rucinski & Fahr (1989) which is appropriate for solar minimum conditions but requires a three-fold increase for solar maximum (Lallement et al. 2004). For this analysis we include a heliographic latitude dependence correction factor, derived from McMullin et al. (2004), that we scale from minimum to maximum. The Lallement et al. (2004) scaling factor in combination with the latitudinal anisotropy factor applied to the Rucinski & Fahr (1989) electron impact model is given in Table 4. An additional simulation (labeled B1) was also performed which was identical to Model B except without electron impact ionization.

The latitude dependence of the solar wind also affects the highly charged heavy ion distribution, where abundances depend on the solar wind type. During minimum solar activity, the solar wind is considered to be highly anisotropic, with a narrow equatorial zone (within $\pm 20°$ of the solar equatorial plane) of slow solar wind with an average speed of $\sim$ 400 km s^{-1} and the fast solar wind emitted from the polar coronal holes at a speed of $\sim$ 700 km s^{-1}. The slow solar wind has a proton density of ~ 6.5 cm^{-3} at 1 AU, while the fast flow is less dense at ~ 3.2 cm^{-3} at 1 AU. At solar maximum, the solar wind spatial distribution is considered to be a complex mix of slow and fast wind states that is in general approximated with an average slow wind flux. The ionic composition of the two flows can be very different with the average oxygen content varying from [O/H] = 1/1780 in the slow wind and [O/H] = 1/1550 in the fast flow. The charge-state distributions change as well, with the higher charge-states strongly depleted (or even completely absent, as for example O^{+8}) in the fast solar wind. For our model we adopt the oxygen relative abundances published in Schwadron & Cravens (2000): (O^{+7}, O^{+8}) = (0.2, 0.07) for the slow wind and (O^{+7}, O^{+8}) = (0.07, 0.0) for the fast wind, based on data from the Ulysses SWICS instrument (Schwadron et al., 2000, unpublished document).

The main difference in the SW heavy ion distribution in our three simulations is the spatial (latitudinal) distribution of the slow and fast solar wind flows. For Model A (minimum SW) the slow SW is expanding in IP space through a $\pm 20°$ equatorial zone on the solar surface, while the fast SW flow occupies the rest of the space. During solar maximum (Model C), we have considered that only an isotropic slow SW flow is present in the IP space. For the late 2003 period (Model B) we assume that there is no fast wind flow in IP space, in order to estimate average upper limits (we also assume that there is no CME or abnormal abundance distributions at the time of the XMM observations) for the resulting SWCX X-ray emission. Indeed, as demonstrated in Koutroumpa et al. (2006, 2007), for high ecliptic-latitude LOS, as is the case for the XMM He cone observations ($\beta \sim -90°$), the oxygen line intensity decreases from solar maximum to solar minimum conditions as the LOS crosses larger fast wind regions where the parent ions are strongly depleted.

The model results for the SEP observations are listed in Table 5. In the same table we list also the HDFN simulation results for Model B.

4. Discussion

4.1. Comparison to *XMM-Newton* data

In Figure 6 we compare the data and model results for the oxygen line intensities for the three *XMM-Newton* observations. We can see that all

TABLE 4
HELIOGRAPHIC LATITUDE DEPENDENT COEFFICIENTS

Hel. Lat. (°)	Model A min (2008)	Model B mid (2003-04)	Model C max (2001)
80	0.6	0.6	2.4
60	0.65	0.65	2.4
40	0.8	0.8	2.7
20	0.9	0.9	2.85
0	1.	1.	3.
-20	0.9	0.9	2.85
-40	0.8	0.8	2.7
-60	0.65	0.65	2.4
-80	0.6	0.6	2.4

NOTE.—Heliographic latitude dependent coefficients scaled for solar activity period to be applied on the Rucinski & Fahr (1989) electron impact ionization rate for He atoms.

TABLE 5
MODEL OXYGEN LINE INTENSITIES IN LU

ObsID	Target	Model A[a]		Model B[b]		Model B1[c]		Model C[d]	
		O VII	O VIII	O VII	O VIII	O VII	O VIII	O VII	O VIII
0162160101	SEP	1.7	0.4	3.3	1.3	3.4	1.3	2.5	1.0
0162160201	HDFN	–	–	3.2	1.3	–	–	–	–
0162160301	SEP	2.4	0.7	3.8	1.5	4.0	1.5	3.0	1.2
0162160401	HDFN	–	–	3.2	1.3	–	–	–	–
0162160501	SEP	1.9	0.5	3.6	1.4	3.8	1.5	2.8	1.1
0162160601	HDFN	–	–	2.9	1.1	–	–	–	–

[a]Minimum solar wind conditions (e.g., 2008).

[b]Medium solar wind conditions (e.g., 2003-04).

[c]Medium solar wind conditions (e.g., 2003-04) with no electron impact ionizations.

[d]Maximum solar wind conditions (e.g., 2001).

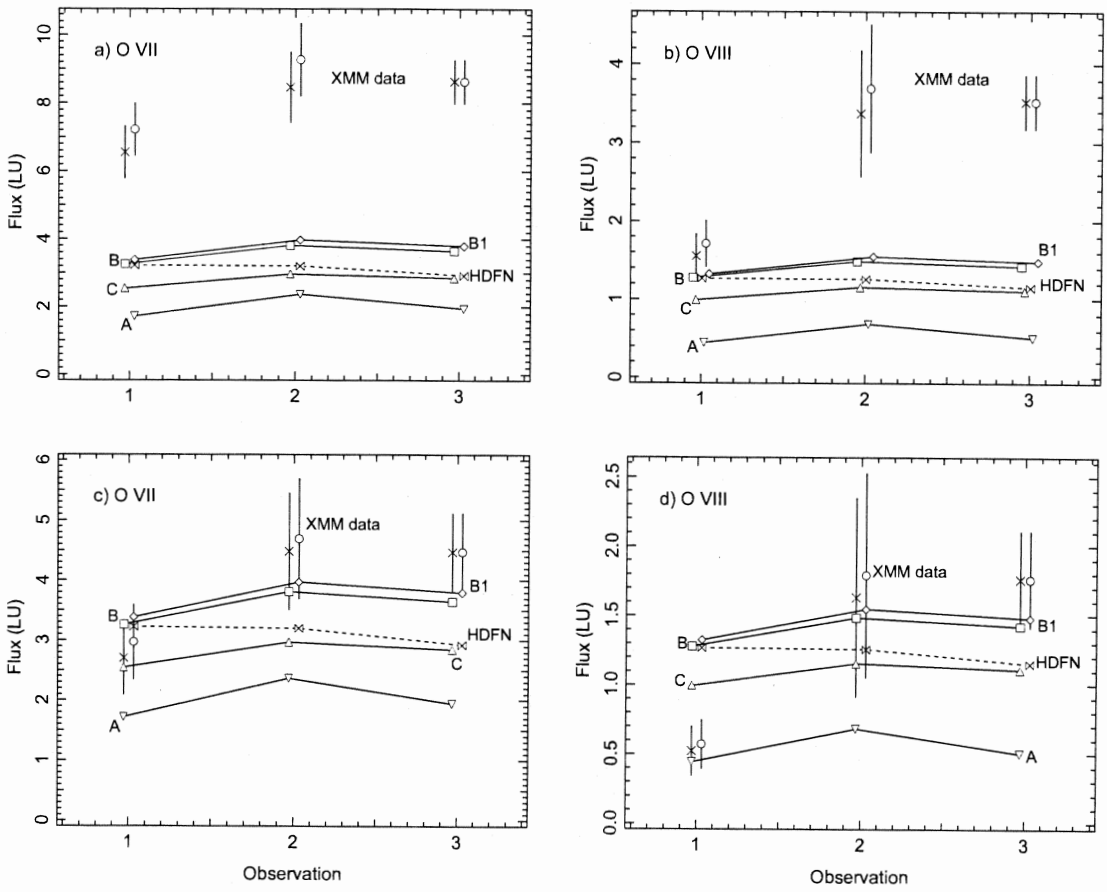

Fig. 6.— a) Model and data line intensities for the O VII triplet. The data are from Table 2. Data points with an X symbol are show the results when the HDFN SWCX flux is assumed to be constant. The points with a circle symbol include a further scaling to account for the model variation in the direction of the HDFN (double-triangle symbol). The model points are from Table 5. Inverse triangle symbols are for Model A, square symbols are for Model B, diamond symbols for Model B1 and triangle symbols are for Model C. b) Same as a) but for the O VIII line. c) and d) are the same as a) and b), respectively, except for the assumption that half of minimum observed flux in both directions has an origin outside of the heliosphere.

the simulations predict the maximum line emission on the second observation date, when the earth is located at 72° of ecliptic longitude. The nominal position of the He cone is at ~75°, only three degrees from the second *XMM-Newton* observation date. We also include the Model B prediction for the HDFN pointings during the observational campaign. If we take into account the HDFN variation predicted in the SWCX model and scale the *XMM-Newton* data we find that the data yield the same trend as the model predictions, although with different relative line strength, both for the first scaling of the data and for where half of the minimum observed emission is assumed to be of cosmic origin.

That the model absolute intensities underpredict the data (when no contribution from the cosmic background is assumed) is not surprising since the observed field is not shadowed from distant emission, such as from the galactic halo. However, assuming that the SWCX emission in the He cone is the only source of variation in the measured data, we should obtain a residual Data (D) - Model (M) cosmic background (here after named R) that is constant over the time. This is not the case either for O VII or for O VIII. In order to have a constant background, that we assume to be equal to the average $D - M$ difference between the three observation dates for each simulation ($R = \mid D - M \mid$), we need to multiply each model point by a correction factor α:

$$\alpha = (D - R)/M, \qquad (1)$$

which we show in Figure 7. Since, neither the average R value representing the residual cosmic background, nor the corrected SWCX emission ($\alpha \cdot M$) are allowed to have negative values, we assume that the average residual cosmic background cannot exceed the lower normalized value detected with *XMM-Newton* for each of the oxygen lines (7.2 and 1.7 LU respectively for O VII and O VIII). A correction factor less than 1 (respectively more than 1) means that the model SWCX emission is overestimated (underestimated) and needs to be lowered (increased) in order to achieve a constant residual background.

If we consider the second data-set, assuming that half of the observed flux is of cosmic origin, then the correction factor may be simplified as α' $= D'/M$, since D' is the residual observed SWCX emission, once the cosmic background has been removed. These correction factors are presented in the lower panels of Figure 7.

From Figure 7 we find that the least correction (best fit) is required for the simulations B/B1 (solar activity ajusted for late 2003) which is in good agreement with the data, especially for the O VII line. The model requiring the largest correction is the one accounting for solar minimum activity period (model A), which assumes a highly anisotropic distribution for the SW oxygen ions. We also see that results for the O VII triplet need smaller corrections than the O VIII results, since the uncertainties both for *XMM-Newton* O VIII data and solar wind data for O^{+8} are very large. Nevertheless, especially when assuming that the oxygen lines are dominated by the SWCX emission from the heliosphere, the correction factor errorbars (calculated based on error propagation from the *XMM-Newton* data standard variations) overlap, revealing that all four models have little differences amongst them, with respect to the absolute differences from the data set.

Our results suggest that toward high ecliptic latitudes in late 2003, there was little fast wind, and a slow wind flux with high oxygen content is required to reproduce the SWCX X-ray increase in the He cone. In order to investigate this assumption, we calculate the correction factors needed by model B to be scaled for different latitudinal extents of the slow solar wind, and we plot the results for line O VII in Figure 8.

Starting at a SW latitudinal extent of ±30° the correction factor progressively improves to its best fit for the three exposures, obtained for an isotropic slow wind (latitudinal extent of ±90° around the solar equator). However, any correction factor variation remains within errorbars, and could eventually be considered non-significant.

4.2. Comparison to *ROSAT* $\frac{1}{4}$ keV data

In Figure 9 we compare the *ROSAT* $\frac{1}{4}$ keV surface brightness as a function of the observation date, with the equivalent SWCX model $\frac{1}{4}$ keV surface brightness. The SWCX simulated spectra toward the North and South ecliptic poles, for each *ROSAT* observation date, were convolved with the *ROSAT* $\frac{1}{4}$ keV band response in order to obtain the surface brightness due to SWCX emission for

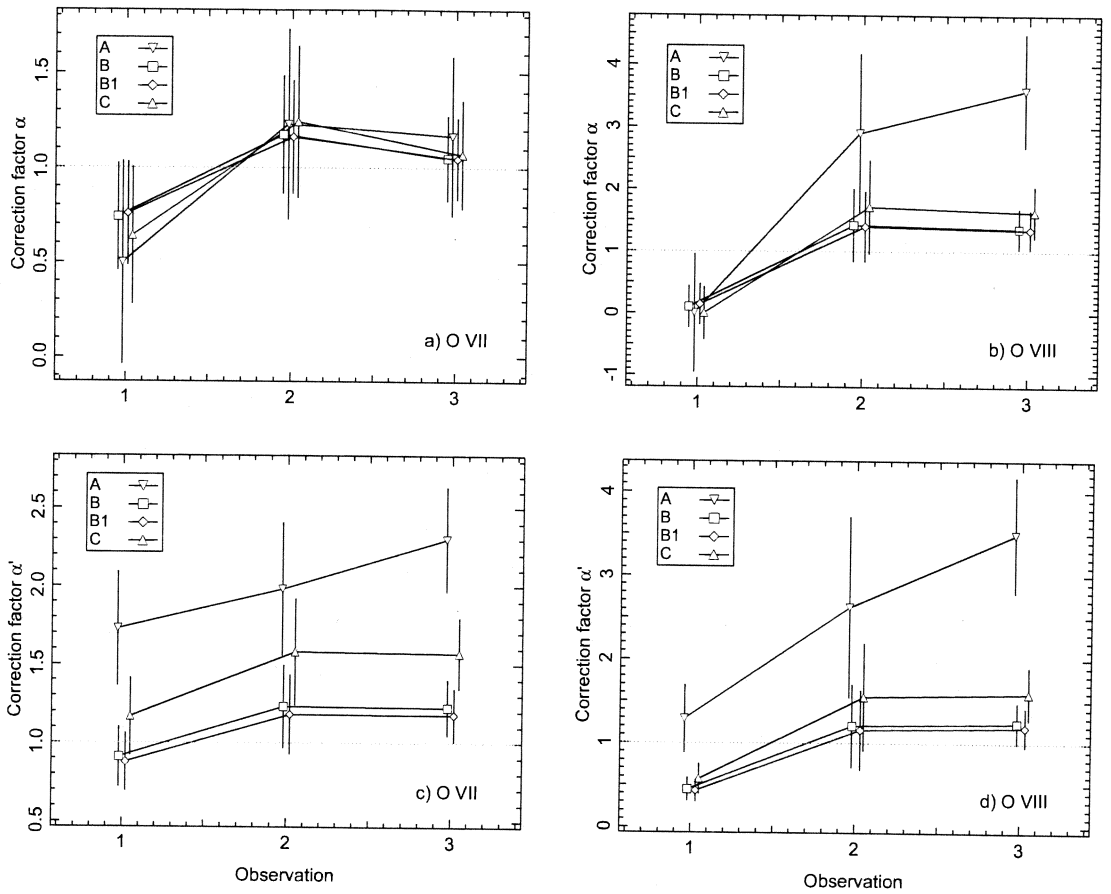

Fig. 7.— a) Correction factor α to apply to the O VII model results in order to obtain a constant data-model difference corresponding to the residual cosmic background assumed this latter is constant. b) Same as a) except for O VIII model results. c) Correction factor α' to apply to the O VII model results in order to match the residual observed SWCX emission, assuming half of the minimum observed flux is of cosmic origin. d) Same as c) except for O VIII. The symbols have the same annotation as in Fig. 6.

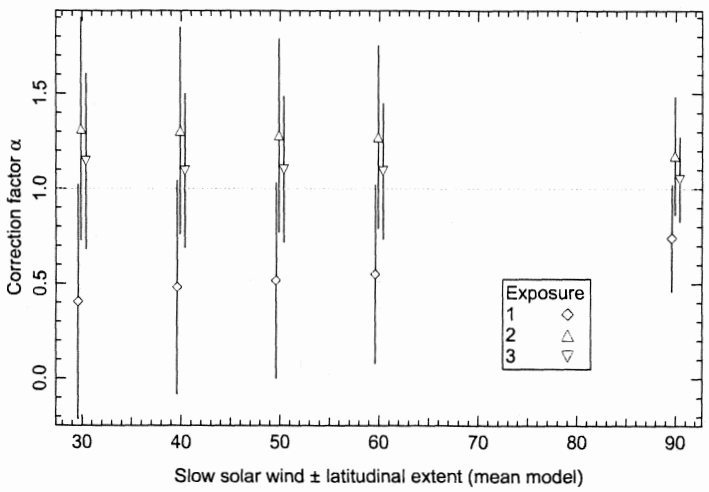

Fig. 8.— Correction factors to apply to model B results for different latitudinal slow SW extent.

these dates and LOS. The first thing to note is that the model shows an expected enhancement for both the SEP and NEP directions. This is not unreasonable as the He cone while centered along a line at -5.5° ecliptic latitude has an angular extent of $\sim \pm 25°$. Comparing the model to the data shows a qualitative agreement with enhancements in the total observed flux (upper curve), also in both directions, and indeed they are the strongest enhancements in terms of their magnitude and duration. The cleaned data (lower curve) indicate that the NEP enhancement was more effectively removed than that for the SEP[3] in the empirical cleaning process. Considering both the cleaned and uncleaned data, the SEP enhancement shows an asymmetry which is seen as a shoulder at higher longitudes. This is a marginal result but is consistent with additional SWCX emission from the secondary He cone. However, this shoulder could also be the effect of a poorly timed enhancement of the solar wind, as the He cone reacts fairly quickly to SW enhancements (see Figures 2 and 5 of Cravens et al. 2001), especially toward polar look directions.

[3]Data from the southern hemisphere were more sparse than from the north as data losses from passage through the South Atlantic Anomaly preferentially affected the south, and this in turn affected the empirical cleaning process.

5. Conclusions

We specifically designed a series of *XMM-Newton* observations in order to observe SWCX emission from the helium focusing cone in the heliosphere. Three observations of the South Ecliptic Pole, coupled with three monitoring observations of the Hubble Deep Field-North were performed. The HDFN observations were used to normalize the SEP data, in order to attempt to eliminate short-term variation effects of the solar wind. We observe a SWCX heliospheric excess (with respect to the off-cone directions) of 2.1±1.3 LU for O VII and 2.0±0.9 LU for O VIII , when we assume that the lines are dominated by SWCX emission from the heliosphere. If we assume that half of the observed emission is of cosmic origin, we find an SWCX excess of 1.7±1.2 LU and 1.2±0.7 LU for O VII and O VIII lines respectively. The maximum emission is observed on the second *XMM-Newton* observation, when the observatory (earth) was located at 72° of ecliptic longitude. This location is consistent with the nominal central position of the He cone (~74°). We find no clear evidence of the secondary He cone reported in Collier et al. (2004), but the data are not inconsistent with such a component either.

We compared the data results to a self-consistent model of the SWCX X-ray emission in the heliosphere, taking into account both H

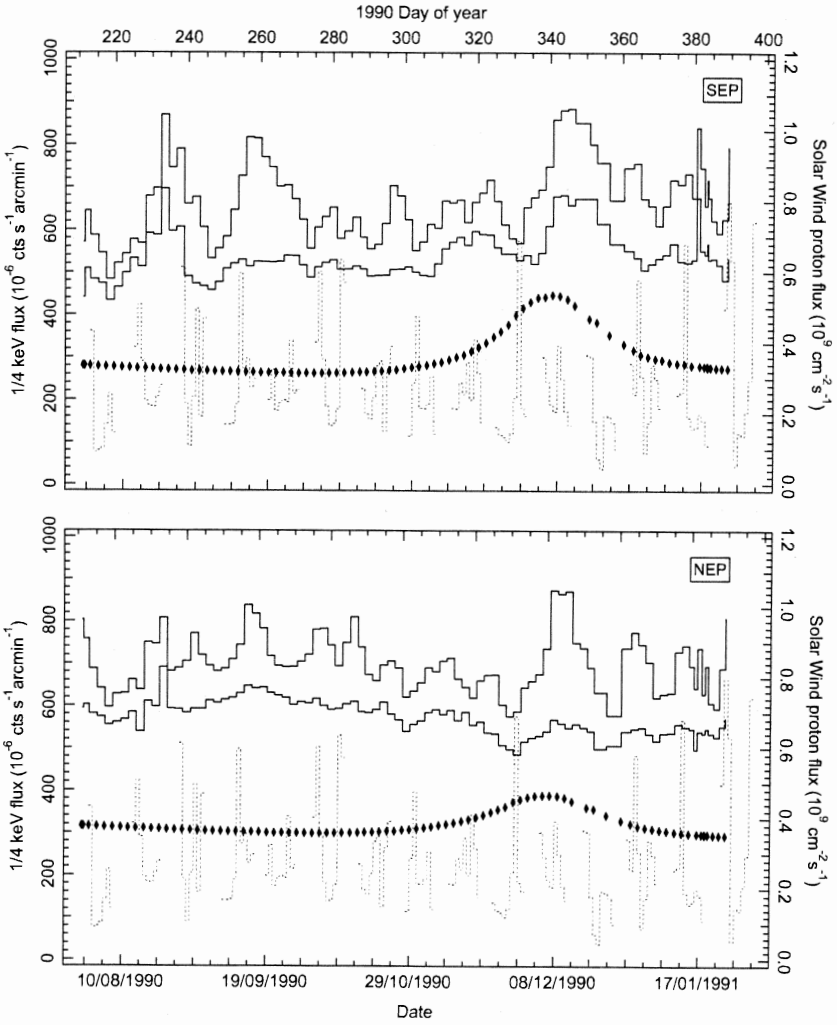

Fig. 9.— *Upper Panel:* Model and data $\frac{1}{4}$ keV surface brightnesses for the south ecliptic pole. The plain curves are the total (upper) and LTE-corrected (lower) RASS $\frac{1}{4}$ keV fluxes. The diamonds are the SWCX model $\frac{1}{4}$ keV fluxes for the same direction. On the right axis (dotted curve) we present daily averages of the solar wind proton flux during the same period. *Lower Panel:* Same as the upper panel except the data and model results are for the north ecliptic pole. Day 366.0 of 1990 is day 1 of 1991.

and He neutral components in the interplanetary space and also accounting for solar activity variations. The model predicted an equivalent trend between the three observations, with the maximum emission occuring at 72° of ecliptic longitude. The average absolute intensity predicted by the model is roughly half of the measured total intensity, since the field of view does not include any shadowing structures (i.e. dense molecular clouds) that would absorb the more distant halo emission. However, the on-cone excess predicted by the model (assuming solar conditions close to the late 2003 period, when the *XMM-Newton* observations were performed) is much smaller with respect to the data on-cone excess, only 0.5 LU and 0.2 LU for O VII and O VIII respectively.

This discrepancy between the model results and the data may be attributed to short-scale solar wind variations that the model was unable to account for. The *ACE* and *WIND* data in the ecliptic plane at 1 AU displayed significant variations during this period, but within reasonable limits. However, considering the high ecliptic latitude observation geometry, both for the SEP and the HDFN pointings, we cannot assert that the solar wind conditions were indeed the same as the ones measured in the ecliptic, or that both the SEP and HDFN observations were influenced by solar wind of the same characteristics. In order to quantify the model to data discrepancy we produced a series of scaling factors needed by the different simulations to match the data. The corection factors for the simulations accounting for the late 2003 period of solar activity show a reasonable agreement of the model with the data.

We also compared a series of RASS data toward the South and North ecliptic poles with the SWCX model results in the $\frac{1}{4}$ keV band. The data (both NEP and SEP) exhibit a clear enhancement near the nominal He cone position predicted in the model. The SEP data also show a shoulder towards higher longitude which may be consistent with the presence of the secondary He cone. However, it must be noted that the shoulder could also be due to a serendipitous enhancement of the solar wind.

More X-ray observations of the He cone, especially during different solar activity periods, are needed to further constrain the SWCX emission from the He cone and the heliosphere in general. Hopefully, the study will be reinforced by spectral diagnostics with the help of future X-ray missions including calorimeter instruments.

The authors wish to thank M. Bzowski for constructive and very useful discussions on the neutral gas distributions.

Based on observations obtained with *XMM-Newton*, an ESA science mission with instruments and contributions directly funded by ESA Member States and NASA.

We are grateful to the ESA *XMM-Newton* SOC for supporting and planning the special calibration observations used in this paper.

This research was supported by an appointment to the NASA Postdoctoral Program at the Goddard Space Flight Center, administered by Oak Ridge Associated Universitites through a contract with NASA.

REFERENCES

Auchère, F., Cook, J. W., Newmark, J. S., McMullin, D. R., von Steiger, R., & Witte, M. 2005, ApJ, 625, 1036

Bzowski, M., Fahr, H. J., & Rucinski, D. 1996, Icarus, 124, 209

Collier, M. R., Snowden, S. L., Moore, T. E., Simpson, D., Pilkerton, B., Fuselier, S., & Wurz, P. 2003, AGU Fall Meeting, #SH11C-1123

Collier, M. R., Moore, T. E., Simpson, D., Roberts, A., Szabo, A., Fuselier, S., Wurz, P., Lee, M. A., & Tsurutani, B. T. 2005, AdSpR, 34, 166

Cox, D. P. 1998, IAU Colloq. 166: The Local Bubble and Beyond, 506, 121

Cravens, T. E. 2000, ApJ, 532, L153

Cravens, T. E., Robertson, I. P., & Snowden, S. L. 2001, J. Geophys. Res., 106, 24883

Frisch, P. C. 2000, J. Geophys. Res., 105, 10279

Gloeckler, G., et al. 2004, A&A, 426, 845

Gruntman, M. A. 1994, J. Geophys. Res., 99, 19213

Holmström, M., Collier, M. R., Barabash, S., Brinkfeldt, K., Moore, T. E., & Simpson, D. 2008, Advances in Space Research, 41, 343

Kharchenko, V., & Dalgarno, A. 2000, J. Geophys. Res., 105, 18351

Kharchenko, V. 2005, AIPC, 774, 271

Koutroumpa, D., Lallement, R., Kharchenko, V., & Dalgarno, A. 2008, Space Sci. Rev., 87

Koutroumpa, D., Acero, F., Lallement, R., Ballet, J., Kharchenko, V. 2007, A&A, 475, 901

Koutroumpa, D., Lallement, R., Kharchenko, V., Dalgarno, A., Pepino, R., Izmodenov, V., Quémerais, E. 2006, A&A, 460, 289

Kuntz, K. D., & Snowden, S. L. 2007, A&A, 478, 575

Moebius, E., Hovestadt, D., Klecker, B., Scholer, M., & Gloeckler, G. 1985, Nature, 318, 426

Lallement, R. 1999, American Institute of Physics Conference Series, 471, 205

Lallement, R., Raymond, J. C., Vallerga, J., Lemoine, M., Dalaudier, F., & Bertaux, J. L. 2004, A&A, 426, 875

Lallement, R., Quémerais, E., Bertaux, J. L., Ferron, S., Koutroumpa, D., & Pellinen, R. 2005, Science, 307, 1447

Lallement, R. 2008, Space Science Reviews, 152

Lisse, C. M., et al. 1996, Science, 274, 205

McMullin, D. R., et al. 2004, A&A, 426, 885

Ogilvie, K. W., et al. 1995, Space Science Reviews, 71, 55

Quémerais, E., Bertaux, J. L., Lallement, R., Berthé, M., Kyrölä, E., & Schmidt, W. 1999, J. Geophys. Res., 104, 12585

Quémerais, E., Lallement, R., Ferron, S., Koutroumpa, D., Bertaux, J. L., Kyrölä, E., & Schmidt, W. 2006, J. Geophys. Res. (Space Physics), 111, 9114

Robertson, I. P., & Cravens, T. E. 2003, Geophys. Res. Lett., 30(8), 1439

Rucinski, D., & Fahr, H. J. 1989, A&A, 224, 290

Schwadron, N. A., & Cravens, T. E. 2000, ApJ, 544, 558

Smith, R. K., Edgar, R. J., Plucinsky, P. P., Wargelin, B. J., Freeman, P. E., & Biller, B. A. 2005, ApJ, 623, 225

Snowden, S. L., Collier, M. R., Cravens, T., Kuntz, K. D. & Robertson, I. 2009, ApJ, in press

Snowden, S. L., Collier, M. R., & Kuntz, K. D. 2004, ApJ, 610, 1182

Snowden, S. L., & Kuntz, K. D. 2006, *XMM-Newton* GOF

Snowden, S. L. 2008, Space Science Reviews, 114

Snowden, S. L., Mushotzky, R. F., Kuntz, K. D., & Davis, D. S. 2008, A&A, 478, 615

Snowden, S. L., et al. 1995, ApJ, 454, 643

Snowden, S. L., Egger, R., Freyberg, M. J., McCammon, D., Plucinsky, P. P., Sanders, W. T., Schmitt, J. H. M. M., Truemper, J., & Voges, W. 1997, ApJ, 485, 125

Stone, E. C., Frandsen, A. M., Mewaldt, R. A., Christian, E. R., Margolies, D., Ormes, J. F., & Snow, F. 1998, SSRv, 86(1/4), 1

Vallerga, J., Lallement, R., Lemoine, M., Dalaudier, F., & McMullin, D. 2004, A&A, 426, 855

Wang, L., Lin, R. P., Larson, D. E., & Luhman, J. G., 2008, AGU Fall Meeting Abstracts, A5

Witte, M. 2004, A&A, 426, 835

Woods, T. N., Tobiska, W. K., Rottman, G. J., & Worden, J. R. 2000, J. Geophys. Res., 105, 27195

Wurz, P., Collier, M. R., Moore, T. E., Simpson, D., Fuselier, S., & Lennartson, W. 2004, Physics of the Outer Heliosphere, 719, 195

This 2-column preprint was prepared with the AAS LaTeX macros v5.2.